SPECTRAL ABSORPTION COEFFICIENT OF ADDITIVE MANUFACTURING POLYMERS

Nicholas J. Wallace, Matthew R. Jones, Nathan B. Crane

Brigham Young University
Ira A. Fulton College of Engineering,
Provo, Utah 84602

ABSTRACT

As NASA turns to additive manufacturing processes, there is a need to ensure that the parts they produce are reliable. This is especially true when creating parts in space, where resources are limited and failure could result in catastrophe. Active thermography has shown potential as a non-destructive quality assurance technique for additive manufacturing processes. Heat transfer models used in active thermography techniques require accurate material property measurements in order to extract useful information about the system, including defect location. The spectral absorption coefficient, which determines the depth at which radiative power is absorbed into a surface, is a material property necessary for performing active thermography on AM polymers. This paper presents measurements of spectral absorption coefficients of polymers commonly used in additive manufacturing. Spectral absorption coefficients for fully dense PLA, ABS, and Nylon 12 samples are reported. Future work is needed to measure the spectral absorption coefficients of different materials and colored filaments commonly used in additive manufacturing.

NOMENCLATURE

AM	additive manufacturing
RTE	radiative transfer equation
$\tau_\lambda^{\perp\ominus}$	spectral, normal-hemispherical transmissivity.
$\rho_\lambda^{\perp\ominus}$	spectral, normal-hemispherical reflectivity
κ_λ	spectral absorption coefficient
ρ_λ	spectral reflectivity
t	sample thickness
I_λ	spectral intensity
α	absorptivity

1. INTRODUCTION

Innovative, reliable and lightweight systems capable of sustaining life in harsh environments are required for NASA's missions of establishing permanent operational bases on the Moon and Mars [1]. Additive manufacturing (AM) is key to the success of these plans by allowing crew members to adapt designs and create parts and supplies as needed. In addition, relying on AM processes could decrease payload weight by eliminating redundant equipment being carried into space. This is especially true if material is recycled for AM fabrication as demonstrated by NASA's 'refabricator' [2]. AM may also enable the use of in-situ resources by mining raw materials on the Moon and Mars. There is a real need to ensure that NASA's additively manufactured parts are reliable, especially when parts are constructed using materials obtained from in-situ resources or recycling, whose properties are not accurately known.

The hypothesis of this research is that NASA can ensure the quality of their additively manufactured parts through a non-destructive technique called active thermography.

Active thermography is performed by irradiating an object's surface with a pulse, or a series of pulses, and observing the resulting changes in surface temperature, as illustrated in Figure 1. Since thermophysical properties of defects differ from the properties of sound regions, heat transfer models can be used to reveal the location of flaws which are introduced during AM processes [3-14].

There are characteristics of AM which are uniquely advantageous for thermography applications. Because AM is an incremental process, thermography could be performed at each layer while the defects are close to the surface, thus enhancing the ability to accurately assess the integrity of the final part. Furthermore, the same heat sources which sinter AM materials could simultaneously be used to perform thermography between each layer of a print. This efficient use of existing equipment could reduce the cost and increase the efficiency of thermography applications.

There are, however, aspects of traditional thermography techniques which limit its usefulness when applied to AM processes. For instance, the ability to detect small defects in AM through active thermography remains unclear. Existing research seems to focus on large defect sizes (~2-5 cm) that might be representative of large delamination defects [5, 11]. However, even small pores on the order of 100 μm can have significant effects on the integrity of the final part [15, 16]. There is a need to investigate, and quantify the detection threshold of active thermography in AM.
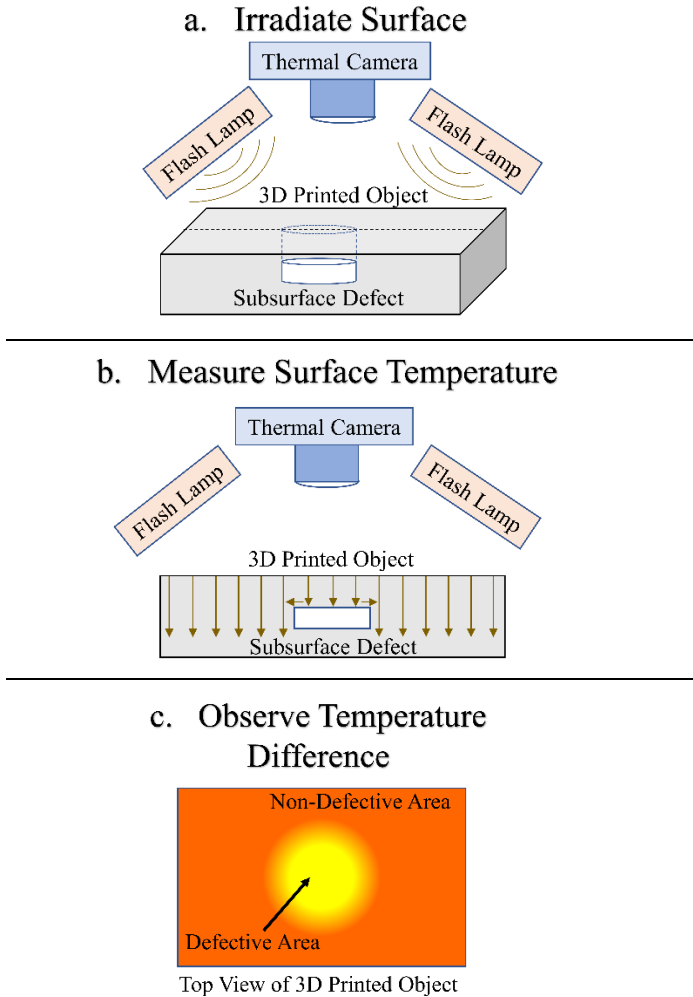
a. Irradiate Surface

b. Measure Surface Temperature

c. Observe Temperature Difference

FIGURE 1: THERMAL RESPONSE OF DEFECTIVE AND NON-DEFECTIVE AREAS AFTER BEING IRRADIATED BY A FLASH LAMP. THE LINES IN (B) REPRESENT A THERMAL WAVE PROPAGATING THROUGH THE OBJECT. AREAS WITH LOW THERMAL CONDUCTIVITY OBSTRUCT THE PROPAGATION OF SUCH WAVES AND CAUSE HIGHER SURFACE TEMPERATURES.

Furthermore, traditional thermography models assume that irradiation is absorbed completely at the surface. This simplification has yielded good results in the past for systems made with materials with large absorption coefficients (such as metals), but many AM processes use polymers with relatively small absorption coefficients. If defects form near the surface, then this increased absorption depth can cause a portion of the irradiation to be transmitted into the material below. These factors distort the surface temperature measurements necessary for active thermography applications [11].

In order to accurately apply active thermography to AM processes, the effects of in-depth adsorption must be considered. The spectral absorption coefficient defines the depth at which radiative power is absorbed by a material. Values of the spectral absorption coefficient in the UV are available in the literature [17, 18], but data in the visible and NIR is sparse. The visible spectrum is of particular interest because a significant portion of the emission from commonly used sources is in the visible spectrum [19, 20]. Thus, measurement of absorption coefficients in the visible spectrum are required to use existing AM equipment for both sintering and active thermography.

2. MATERIALS AND METHODS

The process used to obtain values for the spectral absorption coefficient of typical AM materials is illustrated in Figure 2. In this figure, ρ_λ is the spectral reflectivity, τ_λ is the spectral transmissivity, I_λ is the spectral intensity, and t is the thickness of the semitransparent samples.
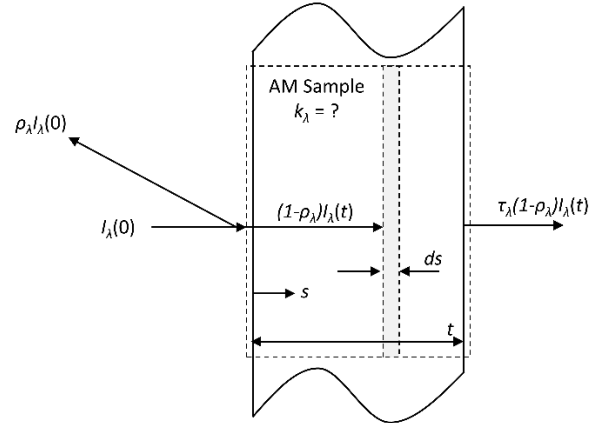

Figure 2: ARBITRARY SYSTEM PARTIALLY REFLECTING, TRANSMITTING, AND ABSORBING IRRADIATION FROM THE LEFT

Applying the Radiative Transfer Equation (RTE) along the path indicated in Fig. 2 gives:

$$\frac{dI_\lambda}{ds} = \kappa_\lambda I_{b\lambda}(T(s)) - \kappa_\lambda I_\lambda - \sigma_{s\lambda} I_\lambda + \frac{\sigma_{s\lambda}}{4\pi} \int_{4\pi} I_\lambda(\hat{s}_i)\Phi(\hat{s}_i, \hat{s})d\Omega_i$$

$$(1)$$

Assuming the material is non-scattering and emission in the visible and IR spectrum is negligible, Eq. 1 simplifies to:

$$\frac{dI_\lambda}{ds} = -\kappa_\lambda I_\lambda \qquad (2)$$

Separating and integrating along the path indicated in Figure 2 yields Equations 3.

$$\ln\left(\frac{I_\lambda(t)}{I_\lambda(0)(1-\rho_\lambda)}\right) = -\kappa_\lambda t \qquad (3)$$

The spectral, normal-normal transmissivity of the material is defined as the ratio of the spectral intensity transmitted directly through the sample to the spectral intensity incident on the sample in the normal direction. Solving Eq. 3 for the spectral, normal-normal transmissivity gives:

$$\frac{I_\lambda(t)}{I_\lambda(0)} = \tau_\lambda = (1 - \rho_\lambda)e^{-\kappa_\lambda t} \qquad (4)$$

Solving Eq. 4 for the spectral absorption coefficient gives:

$$\kappa_\lambda = \frac{\ln\left(\frac{1-\rho_\lambda}{\tau_\lambda}\right)}{t} \qquad (5)$$

A similar process has been shown by Modest and Bergman et al. [21, 22]. Based on Eq. (5), it is seen that the spectral absorption coefficient would need to be calculated from three separate measurements: spectral transmissivity measurements, spectral reflectivity measurements, and sample thickness measurements. An integrating sphere system was used for measuring the spectral transmissivity and spectral reflectivity, whereas a micrometer was used to measure the thickness of ABS, PLA, and Nylon 12 samples as described.

2.1 Transmissivity Measurements

A laser at either 532 or 660 nm was directed into the integrating sphere through a small opening. After entering the sphere, the light was reflected multiple times until eventually absorbed by photodiode. A multimeter was then used to measure the current output of the diode. A polymer sample was then placed in front of the laser's path, and the process was repeated in order to determine the portion of the radiation blocked by the material. The spectral normal-hemispherical transmissivity, $\tau_\lambda^{\perp\cap}$, was determined by finding the ratio between the current reading when the laser was obstructed and the current reading when the laser entered freely into the sphere. This process was repeated for various samples of different thicknesses and materials. The basic process and experimental setup are depicted in Figure 3.

$$\tau_\lambda^{\perp\cap} = \frac{(I_{laser}-I_{dark})_{sample}}{(I_{laser}-I_{dark})_{empty}} \qquad (6)$$

Equation 6 was used to compensate for dark current effects. The subscripts "sample" and "empty" represent current measurements taken when the radiation was obstructed by the

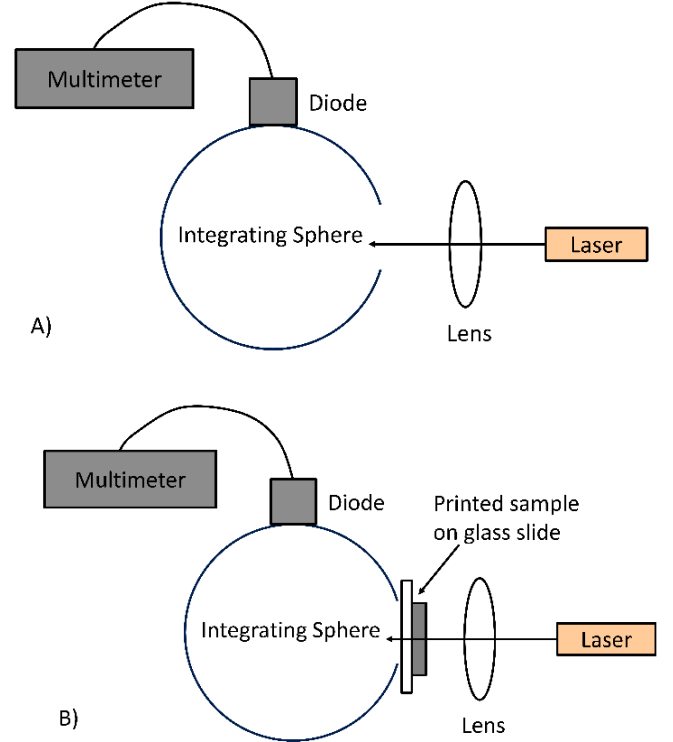sample and current measurements taken when radiation entered freely into the sphere as shown in Figure 3.

Figure 3: BASIC PROCESS FOR SPECTRAL, NORMAL-HEMISPHERICAL TRANSMISSIVITY MEASUREMENTS USING AN INTEGRATING SPHERE. A) RADIATION ENTERS SPHERE UNOBSTRUCTED AND CURRENT IS MEASURED FROM PHOTODIODE. B) RADIATION IS OBSTRUCTED BY SAMPLE AND CURRENT IS READ FROM PHOTODIODE

2.2 Reflectivity Measurements

There are two differences between the process for measuring the spectral, normal-heispherical reflectivity and the spectral, normal-heispherical transmissivity using the integrating sphere. These differences are illustrated in Figure 4. First, the polymer sample was moved to the opposite side of the sphere. In this configuration the laser was allowed to enter the sphere freely, hit the sample mounted on the opposite side, and then partially reflect back into the sphere for current measurements from the photodiode. Second, a reflectance calibration standard was purchased and used for baseline measurements. The reflectivity of this calibration standard was multiplied by the final ratio of current measurements shown in Equation 7.

$$\rho_\lambda^{\perp\cap} = \frac{(I_{laser}-I_{dark})_{sample}}{(I_{laser}-I_{dark})_{calibration\ standard}} * R_{calibration\ standard} \qquad (7)$$

Dark current effects were subtracted from the current measurements as shown in Equation 7. The numerator of this equation represents current measurements taken when the

sample was mounted as shown in Figure 4B. The denominator represents current measurements taken when the calibration standard was mounted as shown in Figure 4A. R represents the reflectivity of the calibration standard.
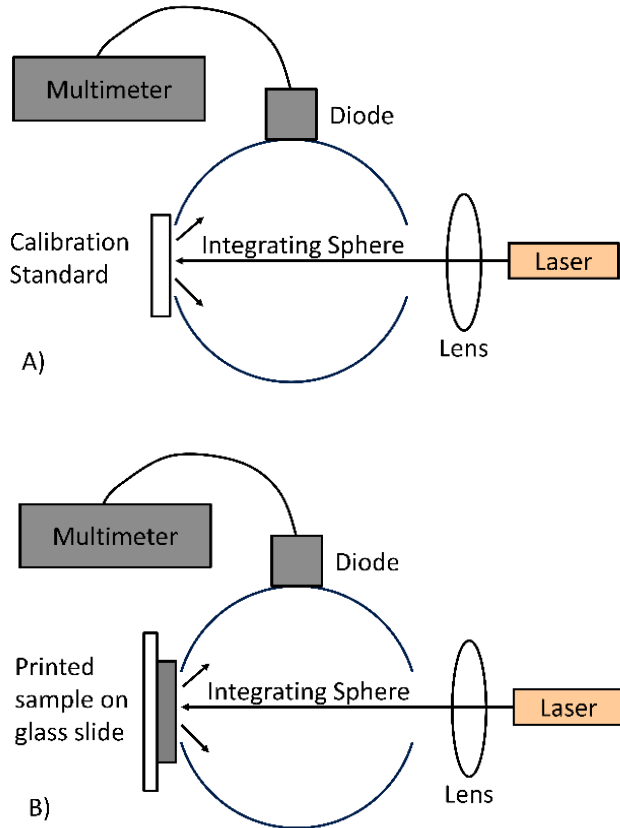

Figure 4: BASIC PROCESS FOR SPECTRAL, NORMAL-HEMISPHERICAL REFLECTIVITY MEASUREMENTS USING AN INTEGRATING SPHERE. A) RADIATION ENTERS SPHERE UNOBSTRUCTED, HITS CALIBRATION STANDARD, AND IS PARTIALLY REFLECTED BACK INTO SPHERE FOR CURRENT MEASUREMENTS B) CALIBRATION STANDARD IS REPLACED WITH SAMPLE

2.3 Sample Creation

Samples of sintered nylon 12 powder, as well as ABS and PLA filaments, were created on 1 mm thick glass slides. The black PLA filament was purchased from Hatchbox, while the black ABS filament was purchased from IC3D. The black PA2202 Nylon 12 powder was purchased from EOS. The samples were created by placing the material on a glass slides and heating them in an oven while a weight rested on top of them. This resulted in the fully dense samples like the ones shown in Figure 5. The transmissivity of the glass slide was measured separately and divided from the final measured transmissivities of the polymer-glass combination. This was intended to compensate for any differences the glass may have made on the final transmissivity measurements.
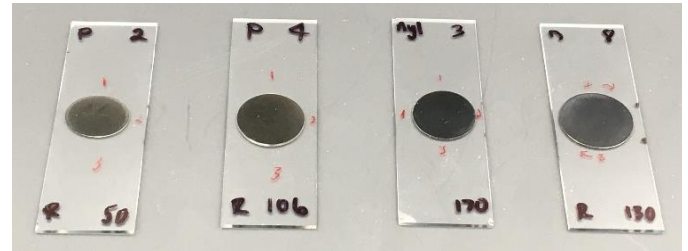

Figure 5: FULLY DENSE PLA AND NYLON SAMPLES USED FOR MEASURING THE SPECTRAL ABSORPTION COEFFICIENT

2.4 Thickness Measurements

Sample thickness was measured using an analog micrometer with a 1.3 μm resolution. Three measurements were averaged together to obtain the thicknesses used in the spectral absorption coefficient measurements.

3. RESULTS

An Agilent Cary-60 spectrometer was used to validate measurements taken with the integrating sphere system. This spectrometer was designed to measure the absorptance of liquid solutions and is primarily used for biological research. Customized hardware was created to hold the polymer samples during transmissivity measurements. Initially, measurements from the two systems did not match, because the Cary-60 spectrometer measures specular transmissivity, whereas the integrating sphere system measures over the entire hemisphere. A "specular exclusion port" (light dump with $\alpha \approx 1$) was installed on the integrating sphere and any transmission not in the direction of the laser was subtracted from the final measurements. Figure 6 shows the comparative transmissivity measurements between the two systems after the "specular exclusion port" was installed. The values retrieved from the two measurement systems lie within the envelope of uncertainty. Measurements from the integrating sphere system were considered validated from these results.

Spectral absorption coefficients at 532 and 660 nm are reported in Table 1 for fully dense ABS, PLA, and Nylon 12 samples. Color and manufacturer are also reported.

Table 1: ABSORPTION COEFFICIENT OF FULLY DENSE AM POLYMERS (μm^{-1})

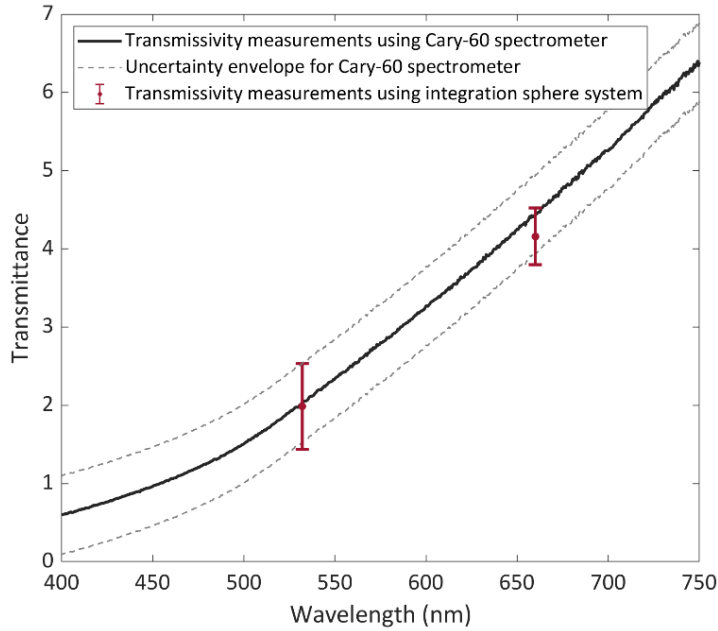| Material	Color	Manufacturer	660 nm	532 nm
PLA	Black	Hatchbox	.022 +/- .002	.026 +/- .003
ABS	Black	IC3D	.025 +/- .003	.028 +/- .005
Nylon 12	Black	EOS	.026 +/- .003	.030 +/- .005

Figure 6: COMPARING SPECTRAL, NORMAL-NORMAL TRANSMISSIVITY MEASUREMENTS FROM A CARY-60 SPECTROMETER AND THE INTEGRATING SPHERE SYSTEM FOR A BLACK, FULLY DENSE PLA SAMPLE 109 MICRONS THICK

Exponentially decaying transmission curves based on the measured spectral absorption coefficients are compared to the transmissivity data retrieved from the integrating sphere system in Figure 7. The fitted curves based on the measured absorption coefficients appear to predict the data well.
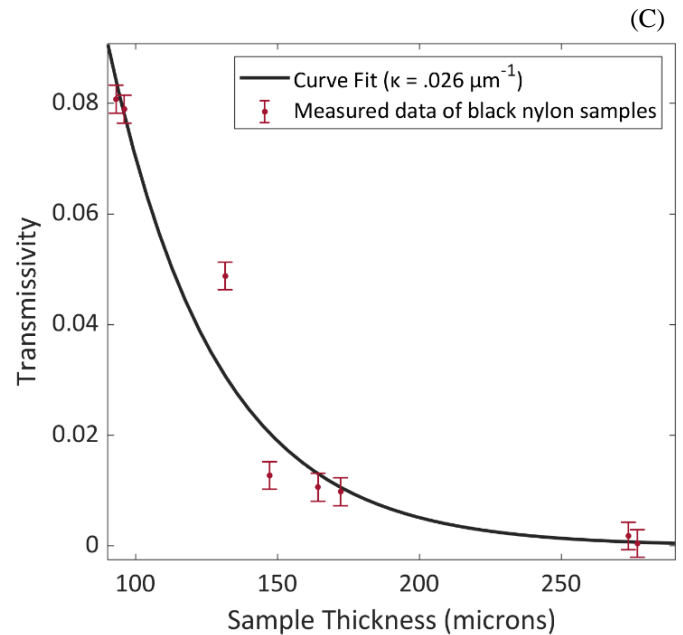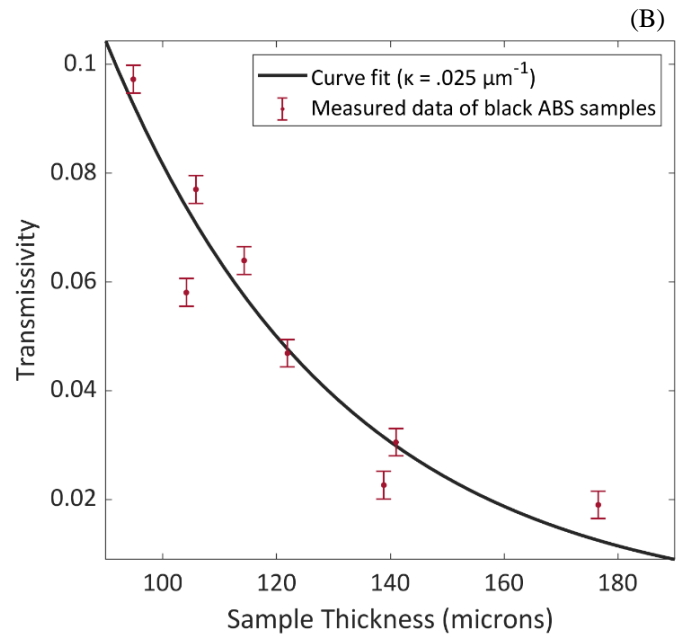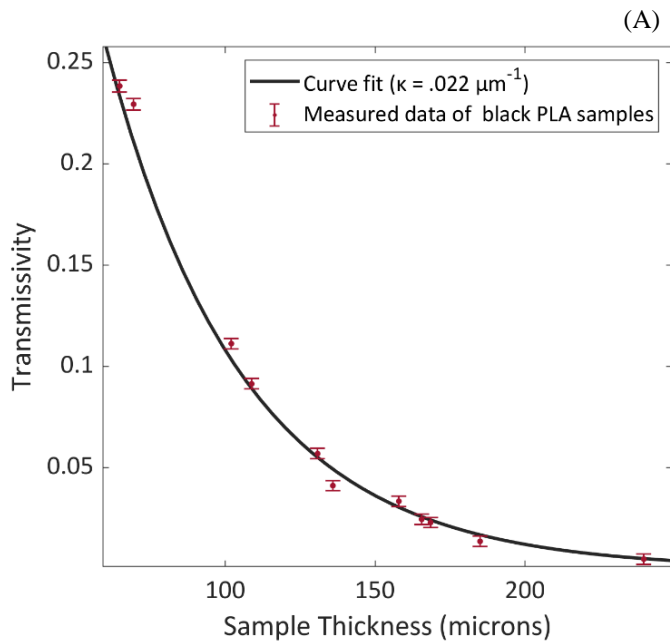

Figure 9: TRANSMISSIVITY OF BLACK, FULLY DENSE PLA (A), ABS (B) AND NYLON 12 (C) SAMPLES IRRADIATED AT 660 NM

4. CONCLUSION AND DISCUSSION

Spectral absorption coefficient measurements at 532 and 660 nm have been presented for black, fully dense PLA, ABS, and Nylon 12 samples. The transmission curves predicted by the measured absorption coefficients appear to coincide with the measured transmissivity data. The values were validated by comparing transmissivity measurements from the Cary-60 spectrometer to transmissivity measurements from the integrating sphere system.

As mentioned in the introduction, AM polymers have significant in-depth absorption which can alter results obtained from traditional thermography techniques. It is anticipated that including in-depth absorption in these existing models will allow active thermography to be a reliable technique for assessing the integrity of an additively manufactured part.

Improving AM processes supports NASA, including their missions to establish operational bases on the Moon and Mars. High-fidelity models that include pertinent parameters (such as accurate in-depth absorption coefficient measurements) could provide NASA the added certainty and flexibility to design and create custom parts in remote locations as needed. By relying on AM, NASA could reduce the amount of redundant equipment carried into space as well as the overall payload weight.

Additional spectral absorption coefficient measurements are needed for different AM materials and colored filaments. In addition, a relationship between sample porosity and the absorption coefficient would be useful since AM processes do not create fully dense parts. Accurate spectral absorption coefficient measurements are necessary to successfully adapt active thermography techniques as a non-destructive, non-contact means of in-situ monitoring of AM processes.

ACKNOWLEDGEMENTS

REFERENCES

1. Dunbar, B., *Moon to Mars Overview.* 2019.
2. Harbaugh, J., *Refabricator to Recycle, Reuse Plastic Installed on Space Station.* 2019.
3. Sun, J.G., *Quantitative Three-Dimensional Imaging of Heterogeneous Materials by Thermal Tomography.* Journal of Heat Transfer-Transactions of the Asme, 2016. **138**(11).
4. Sun, J.G., *Analysis of pulsed thermography methods for defect depth prediction.* Journal of Heat Transfer-Transactions of the Asme, 2006. **128**(4): p. 329-338.
5. Pierce, J.R. and N.B. Crane, *Preliminary Nondestructive Testing Analysis on 3d Printed Structure Using Pulsed Thermography.* Proceedings of the Asme International Mechanical Engineering Congress and Exposition, 2017 Vol 8, 2018.
6. Pierce, J.a.N.B.C., *Impact of pulse length on the accuracy of defect depth measurements in pulse thermography.* Journal of Heat Transfer-Transactions of the Asme, 2019. **141**(4).
7. Metz, C., Franz, P., Fischer, C., Wachtendorf, V., Maierhofer, C. , *Active thermography for quality assurance of 3D-printed polymer structures* 14th Quantitative InfraRed Thermography Conference, 2018.
8. Maldague, X., F. Galmiche, and A. Ziadi, *Advances in pulsed phase thermography.* Infrared Physics & Technology, 2002. **43**(3-5): p. 175-181.
9. Maldague, X., Marinetti, S., *Pulse phase infrared thermograph.* Journal of Applied Physics, 1996. **79**(2694).
10. Lau, S.K., D.P. Almond, and J.M. Milne, *A quantitative analysis of pulsed video thermography.* NDT & E International, 1991. **24**(4): p. 195-202.
11. Bernegger, R., Altenburg, S. J., Maierhofer, C., *Quantifcation of Delaminations in Semitransparent Solids Using Pulsed Thermography and Mathematical 1D Models.* International Journal of Thermophysics, 2020. **41**(67).
12. Parker, W., Jenkins, R., Abbott, G., Butler, C., *Flash Method of Determining Thermal Diffusivity, Heat Capacity, and Thermal Conductivity.* Journal of Applied Physics, 1961. **32**(9): p. 1679-&.
13. Busse, G., D. Wu, and W. Karpen, *Thermal Wave Imaging with Phase Sensitive Modulated Thermography.* Journal of Applied Physics, 1992. **71**(8): p. 3962-3965.
14. Ibarra-Castanedo, C., J.R. Tarpani, and X.P.V. Maldague, *Nondestructive testing with thermography.* European Journal of Physics, 2013. **34**(6): p. S91-S109.
15. Yadollahi, A., Shamsaei, N., Thompson N., Elwany A., Bian L., *Effects of building orientation and heat treatment on fatigue behavior of selective laser melted 17-4 PH stainless steel.* International Journal of Fatigue, 2016. **94**((2017)): p. 218–235.
16. Sanaeia , N., Fatemiab, A., Phanc, N, *Defect characteristics and analysis of their variability in metal L-PBF additive manufacturing.* Materials & Design, 2019. **182**.
17. Barzic, A.I., Barzic R.F., *Optical properties of polysaccharide/polylactide blends.* UPB Sci Bull Ser A, 2015. **77**(4): p. 293-302.
18. Squires, A.D., Lewis, R. A., *Mechanical and optical viability of eighteen filaments for 3D printing of terahertz components.* 42nd International Conference on Infrared, Millimeter, and Terahertz Waves, 2017: p. 1-2.
19. Heather J. O'Connor, A.N.D., Denis P. Dowling,, *Evaluation of the mechanical performance of polymer parts fabricated using a production scale multi jet fusion printing process,.* Additive Manufacturing,, 2018. **Volume 22,**(2214-8604,): p. Pages 381-387,.
20. Nussbaum, J., Crane, B.,, *Evaluation of processing variables in polymer projection sintering.* Rapid Prototyping Journal, 2018(1355-2546).
21. Modest, M.F., *Radiative Heat Transfer.* New York: Academic Press, 2013.
22. Bergman, T.L., Lavine, A. S., Incropera, F. P., Dewitt, D. P. , *Fundamentals of Heat and Mass Transfer.* John Wiley & Sons, Inc., 2002. **Seventh Edition**: p. 896-898.